Characterizing Venus's clouds and hazes using CO_2 absorption bands in flux and polarization 1. Numerical simulations

Gourav Mahapatra[1], Loïc Rossi[2], and Daphne M. Stam[1]

[1]Faculty of Aerospace Engineering, Delft University of Technology, Delft, The Netherlands
[2]CNRS/INSU, LATMOS-IPSL, Guyancourt, France

Key Points:

- Behavior of total and polarized fluxes reflected by Venus like atmosphere has been studied in strong CO_2 absorption bands.
- Polarized flux shows higher sensitivity to Venus cloud and haze particle properties and structure as compared to total flux in these absorption bands.
- An accurate spectro-polarimeter on-board a space mission would provide valuable and independent information on Venus's clouds and hazes.

Corresponding author: Gourav Mahapatra, G.Mahapatra@tudelft.nl

Abstract
Retrievals of Venus cloud top altitudes have primarily been performed using measurements of the total flux of sunlight that is reflected by the planet across CO_2 absorption bands. Linearly polarized fluxes are known to be more sensitive to the properties of clouds and overlying hazes than the total flux. Here, we present results of computations of total and polarized fluxes of reflected sunlight in the wavelength region between 1.4 and 1.5 μm, which covers a strong absorption band of CO_2. We perform an analysis of the sensitivity of the strength and shape of the absorption band in polarization to the vertical distribution of the cloud and hazes particles, i.e. cloud top altitude, and cloud and haze scale heights, and illumination geometries. We show that the reflected polarization signal at different locations and thus strengths of the absorption band, can help to retrieve more information about the scattering particles in the planetary atmosphere than the total flux alone can. Spectropolarimetry from a Venus orbiter should provide invaluable and independent information into the properties of Venus's clouds and hazes.

Plain Language Summary

Venus is shrouded by thick clouds with their tops varying slightly depending upon location on the planet. Measuring the cloud tops and structure is important to understand the physical processes that are at play in Venus's atmosphere. The cloud tops have previously been measured through satellite instruments measuring the reflected light from Venus's orbit. When light interacts with the atmospheric particles (including cloud particles), it gets polarized. Here we use computer models to show that the polarization of reflected light is highly sensitive to the kind of particles it interacts with, in the atmosphere. The dominant carbon-dioxide gas present in Venus's atmosphere absorbs light at certain wavelengths. We show that measuring the polarized light at these strong absorbing wavelengths of light can provide invaluable information about the structure of the thick cloud layer and the smaller haze particles that are present above the clouds, but are quite challenging to detect through direct reflection of light.

1 Introduction

Already in the 17th century, Christiaan Huygens suggested that Venus was completely covered by clouds, because his telescope would not reveal any spatial variability across the planet due to surface inhomogeneities. Venus's extreme pressures and temperatures sustain layers of sulphuric acid clouds (Hansen & Hovenier, 1974) above 50 km of altitude, spanning a vertical range of 45 to 70 km. The clouds strongly influence Venus's radiative balance, and characterizing their structure and micro-physical particle properties, and the temporal and spatial variations therein is key to understanding the planet's evolution and current climate. While the clouds are ubiquitous, observations with ground-based telescopes, and especially with instruments on dedicated Venus orbiters, such as NASA's Pioneer Venus (1978-1992), ESA's Venus Express or VEx (2006-2014), and JAXA's Akatsuki (launched in 2010, in orbit since 2015), have revealed the clouds' high spatial and temporal variability (Kawabata et al., 1980; Knollenberg & Hunten, 1980; Ignatiev et al., 2009; Fedorova et al., 2016).

Our aim in this paper is to investigate the variation of the reflected solar flux F and in particular the degree of linear polarization P across the CO_2 absorption band around 1.45 μm due to variations in clouds and hazes. Absorption bands of CO_2 have been used for determining Venus's cloud top altitudes, because CO_2 is well-mixed. Ignatiev et al. (2009) analyzed F measurements by the VIRTIS-M instrument (Drossart et al., 2007) on-board ESA's Venus Express (VEx) orbiter (Svedhem et al., 2009; Titov et al., 2006) and found that the cloud top altitude is remarkably constant at about 74 $\pm$ 1 km across most of the planet. Cloud top altitudes (defined at 1.6 μm) decrease poleward of $\sim$50° latitude, towards 65-68 km in the polar regions (Ignatiev et al., 2009). Fedorova et al.

(2016) derived the cloud top altitudes and the water vapor (H_2O) column above the clouds using SPICAV (Bertaux et al., 2007) on the same VEx orbiter, with measurements over a longer time span. They focused on the 1.346 – 1.5 μm wavelength region, that contains both H_2O and CO_2 absorption bands. They derived cloud top altitudes at about 70 km for latitudes between 40° S to 40° N, and a sharp decrease down to 62 km with increasing latitude. Both Ignatiev et al. (2009) and Fedorova et al. (2016) neglected in their analysis the sub-micron haze particles that are known to be present above the clouds, up to at least 90 km, since these particles have a negligible effect on the measured reflected fluxes at these long wavelengths.

We are especially interested in the degree of polarization P across CO_2 absorption bands, because polarimetry is known to be a powerful remote-sensing tool. Hansen and Hovenier (1974) analyzed disk-integrated polarization measurements of Venus in a number of spectral bands and over a broad planet phase angle range to derive the composition (75% H_2SO_4), effective radius (1.05 μm), and effective variance (0.07) of the droplets of the upper clouds. The main reason why these cloud parameters could not be derived from the planet's phase curve in flux is that the variation of P of the reflected light with the phase angle is much more sensitive to particle microphysical properties than the flux is.

The polarization of reflected sunlight across a gaseous absorption band is known to depend on the composition and vertical structure of a planetary atmosphere. Stam et al. (1999) computed P of sunlight reflected by or transmitted through the Earth's atmosphere across the O_2 A-band (which is centered around 765 nm). For the reflected light, they found that P in the band not only depends on the fraction of singly scattered light to multiple scattered light, but also on the vertical distribution of different types of scatterers. Indeed, with increasing atmospheric absorption optical thickness, the fraction of singly scattered light increases, which usually increases $|P|$, and the altitude at which most of the reflected light has been scattered increases, which can either increase or decrease $|P|$, depending on the local single scattering matrix.

A high-resolution polarization spectrum of Venus was measured by Forbes and Fymat (1974) using a ground-based Fourier spectropolarimeter. Numerous fine lines in P across the 1.6 μm CO_2 absorption band are visible in their spectrum. NASA's Pioneer Venus mission carried the Orbiter Cloud PhotoPolarimeter (OCPP) (Travis, 1979), with which the haze above Venus's main cloud deck was detected, and with which the increase of the haze optical thickness towards the poles was found. OCPP, however, measured polarization in a few broad spectral bands. Unfortunately, no space mission targeting Venus has carried a dedicated spectropolarimeter for measuring P across absorption bands. While the SPICAV instrument (Korablev et al., 2012) onboard VEx was designed as a spectrometer, it could (partly) measure polarization because it employed an acousto-optic tunable filter (AOTF) technique with two channels that were sensitive to perpendicularly polarized fluxes. However, because SPICAV was not explicitly calibrated for such measurements, the accuracy of its polarization measurements is limited (Korablev et al., 2012). Rossi et al. (2015) provided a preliminary analysis of SPICAV polarimetric data and derived cloud particle composition and haze optical thicknesses that agree well with values derived from other types of data.

The analysis by Rossi et al. (2015) was done at continuum wavelengths. In this paper, we use radiative transfer computations to investigate the behaviour of total and polarized fluxes of sunlight reflected by Venus's atmosphere across near-IR wavelength bands with strong CO_2 absorption lines, with the focus on the wavelength region from 1.4 to 1.5 μm, where there is a strong variation of absorption line strengths.

The outline of this paper is as follows. In Sect. 2, we provide a description of our numerical algorithm, including the parameters of the model atmospheres. In Sect. 3, we show computed reflected fluxes and polarization across the 1.45 μm CO_2 absorption band

for different model atmospheres, illumination angles, and spectral resolutions. In Sect. 4, we discuss the influence of the spectral resolution of an instrument on the information that spectropolarimetric measurements across this CO_2 absorption band could provide on the composition and structure of the Venusian atmosphere. And in Sect. 5, we present our conclusions. To efficiently compute F and P across the band, we use the correlated k-distribution method or ck-method (Lacis et al., 1992; Fu & Liou, 1992; Stam et al., 2000), which is fast but approximating when combined with scattering. In Appendix A, we present the errors in our computed fluxes and polarization due to using the ck-method.

2 Description of our numerical algorithm

2.1 Definitions of fluxes and polarization

We use Stokes (column) vectors to describe the incident and reflected sunlight (Hansen & Travis, 1974) as follows

$$\mathbf{F}(\lambda) = [F(\lambda), Q(\lambda), U(\lambda), V(\lambda)], \tag{1}$$

with F the total flux, Q and U the linearly polarized fluxes, and V the circularly polarized flux, all with dimension $\mathrm{W/m^2}$ and dependent on the wavelength λ. We assume the sunlight that is incident on Venus to be unidirectional and unpolarized (Kemp et al., 1987, e.g.), such that $\mathbf{F}_0 = F_0[1,0,0,0] = F_0\mathbf{1}$, with πF_0 the incident flux measured perpendicularly to the direction of propagation of the light. Fluxes Q and U of light that is reflected by a specific location on the planet are defined with respect to the local meridian plane. This plane contains the directions towards the local zenith and the observer.

Because our model atmosphere is horizontally homogeneous (see Sect. 2.3), U will be zero with respect to the local meridian plane. Furthermore, in our computations, we ignore V, because it is very small and hardly influences the accuracy of the computation of the total and linearly polarized fluxes (Stam & Hovenier, 2005; Rossi & Stam, 2018). We thus define the degree of polarization P of the light as

$$P(\lambda) = -\frac{Q(\lambda)}{F(\lambda)}. \tag{2}$$

When $P > 0$ ($P < 0$), the direction of polarization is perpendicular (parallel) to the reference plane (i.e. the local meridian plane).

2.2 The radiative transfer algorithm

We compute the sunlight that is reflected by Venus's atmosphere with an adding-doubling algorithm (de Haan et al., 1987) that fully includes polarization for all orders of scattering. The optical properties of the atmospheric layers are described in Sect. 2.3.

Figure 1 shows the illumination and viewing geometries. The local illumination direction is given by θ_0, the angle between the direction to the sun and the local vertical, and ϕ_0, the azimuthal angle of the incident sunlight measured from a given vertical plane. The local reflection direction, i.e. the light that is received by the observer (e.g. an instrument onboard an orbiter), is described by θ, the angle between the direction to the observer and the local vertical, and ϕ, the azimuthal angle of the reflected light. Because our model atmospheres are rotationally symmetric around the local vertical, only the azimuthal angle difference $\phi - \phi_0$ is important, and we define it such that $\phi - \phi_0 = 0°$ (180°) when the propagation directions of the incident sunlight and the reflected light are in the same (other) half of the local vertical plane. The local phase angle α is the angle between the directions to the sun and to the observer.

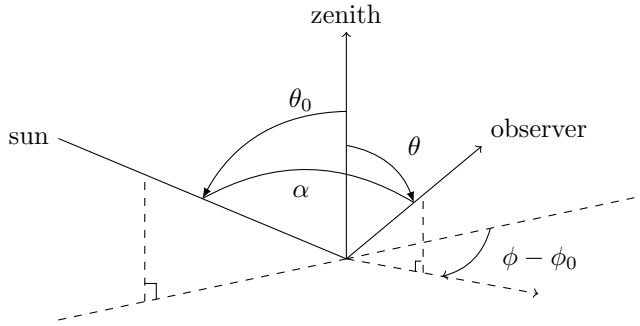

Figure 1. Geometries of the incident and reflected/observed light: local phase angle α, local solar zenith angle θ_0, local reflection angle θ, and local azimuthal difference angle $\phi - \phi_0$.

2.3 The model atmosphere

The model atmosphere is composed of a stack of horizontally homogeneous layers that contain CO_2 gas, and, optionally, cloud or haze particles. It is bounded below by a black surface (because of the thickness of the atmosphere, the reflected light is virtually insensitive to the surface reflection properties). Our adding-doubling algorithm (de Haan et al., 1987) requires for each atmospheric layer: the (average) single scattering matrix, the (average) single scattering albedo, and the total optical thickness. The total optical thickness of an atmospheric layer is the sum of the layer's scattering and absorption optical thicknesses $b_{\rm sca}$ and $b_{\rm abs}$ as follows

$$b(\lambda) = b_{\rm sca}(\lambda) + b_{\rm abs}(\lambda) = b^{\rm m}_{\rm sca}(\lambda) + b^{\rm a}_{\rm sca}(\lambda) + b^{\rm m}_{\rm abs}(\lambda) + b^{\rm a}_{\rm abs}(\lambda), \tag{3}$$

with superscripts 'm' and 'a' denoting the gas molecules and the aerosol particles (i.e. the cloud or haze particles), respectively.

Given a wavelength λ, we calculate $b^{\rm m}_{\rm sca}$ of atmospheric layer i according to

$$b^{\rm m}_{\rm sca}(\lambda) = \frac{24\pi^3}{\lambda^4 N_{\rm L}^2} \frac{(n^2(\lambda)-1)^2}{(n^2(\lambda)+2)^2} \frac{(6+3\rho_n(\lambda))}{(6-7\rho_n(\lambda))} \frac{N_{\rm av}}{R} \int_{z_i}^{z_{i+1}} \frac{p(z)}{T(z)} dz, \tag{4}$$

where $N_{\rm L}$ is Loschmidt's number, n is the refractive index of the gaseous atmosphere, which we assume to consist entirely of CO_2. We assume $n = 1.0004$ between 1.4 and 1.5 μm (Bideau-Mehu et al., 1973). $N_{\rm av}$ is Avogadro's number, and R the universal gas constant. We use a depolarization factor, ρ_n, of 0.09, which is representative for CO_2 (see Hansen & Travis, 1974). Furthermore, p is the ambient pressure, T the ambient temperature, and z_i and z_{i+1} are the altitudes at the bottom and top of the ith atmospheric layer, respectively. Figure 2 shows the vertical profiles of p and T for a latitude of 30°, as taken from the Venus International Reference Atmosphere (VIRA) model (Seiff et al., 1985). The geometric thickness of the layers is 4 km until an altitude of 40 km, and 1 km beyond. In total, the model has 71 layers.

The gaseous absorption optical thickness, $b^{\rm m}_{\rm abs}$, of atmospheric layer i is calculated according to

$$b^{\rm m}_{\rm abs}(\lambda) = \frac{N_{\rm av}}{R} \int_{z_i}^{z_{i+1}} \frac{p(z)}{T(z)} \sigma^{\rm m}_{\rm abs}(\lambda, z) dz, \tag{5}$$

where $\sigma^{\rm m}_{\rm abs}$ is the gaseous absorption cross-section (in cm^{-2}) at the ambient pressure and temperature and the given wavelength, which we calculate using absorption line strengths from the HITRAN 2016 database (Gordon et al., 2017). Fig. 3 shows the atmospheric absorption optical thickness ($b^{\rm m}_{\rm abs}$ summed for all layers) across the wavelength region of our interest. For comparison, the atmosphere's gaseous scattering optical thickness has also been included.

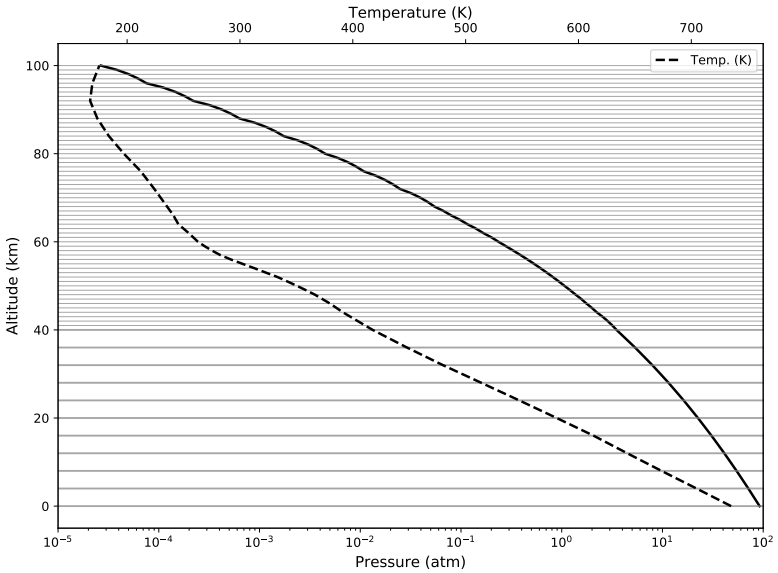

Figure 2. The pressure (solid line) and temperature (dashed line) profiles across our Venus model atmosphere (Seiff et al., 1985), with the horizontal lines showing the geometrical thicknesses of the layers, i.e. 4 km below and 1 km above 40 km altitude.

We use the correlated k-distribution method (the 'ck-method') (Lacis & Oinas, 1991; Fu & Liou, 1992; Stam et al., 2000), for efficient computations of the flux and polarization across the CO_2 absorption band for different spectral instrument response functions, such as that of the SPICAV instrument (Korablev et al., 2012). In the ck-method, strongly wavelength dependent absorption cross-sections are redistributed according to their strength over the spectral region under consideration, such that the integrated flux and polarization signals over that spectral region can be computed with only a few abscissae instead of with numerous line-by-line computations resolving the line spectrum.

A key assumption in the ck-method is that the absorption line strengths are correlated in the spectral domain. In particular in the presence of scattering, this assumption leads to errors in the computed reflected fluxes and polarization. These errors will depend on the vertical variation of the absorption cross-sections, on the spectral region under consideration (the central wavelength and the shape of the spectral response function, e.g. the width of a Gaussian response function), and on the vertical distribution of the scattering particles (Stam et al., 2000).

In Appendix A, we present and discuss the errors due to the assumptions of the ck-method for the numerical simulations presented in this paper. For our simulations, the relative errors in the reflected total and polarized fluxes are smaller than about 12 %, while the absolute errors in the degree of polarization are typically smaller than 1 %. The largest errors are found in the spectral region between 1.435 and 1.45 μm, where the strongest lines are.

The aerosol properties

The aerosol optical thickness b^{a} of atmospheric layer i is computed using

$$b_i^{\mathrm{a}}(\lambda) = \sigma_{\mathrm{ext}}^{\mathrm{a}}(\lambda) N_i^{\mathrm{a}}, \tag{6}$$

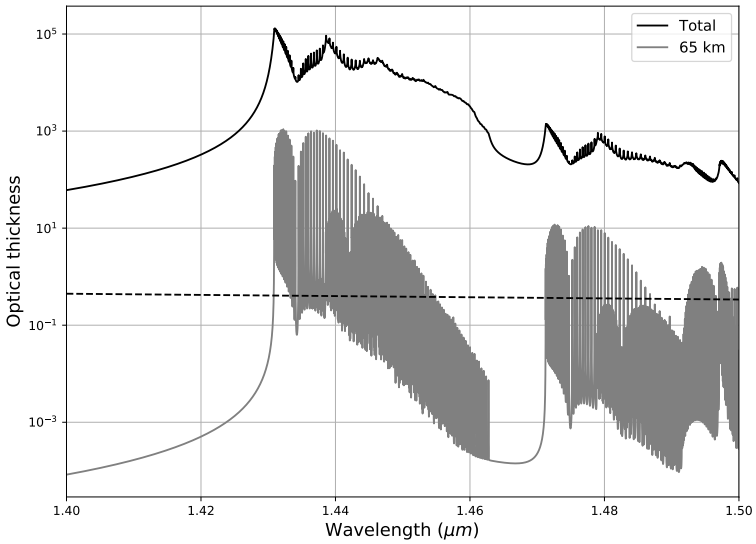

Figure 3. Atmospheric gaseous absorption optical thickness (upper solid line), the gaseous absorption optical thickness of a 2-km thick atmospheric layer around 65 km altitude (lower solid line), and the atmospheric gaseous scattering optical thickness (dashed line).

with $\sigma^{\rm a}$ the aerosol extinction cross–section (in cm^2), and $N_i^{\rm a}$ the aerosol number density in the layer (in cm^{-3}). The extinction cross-section $\sigma_{\rm ext}^{\rm a}$, the single scattering albedo $a^{\rm a}$, and the single scattering matrix $\mathbf{P}^{\rm a}$ of the cloud and haze particles are computed using a Mie-algorithm (De Rooij & Van der Stap, 1984). We thus assume spherical and homogeneous particles. The refractive index for both the cloud and haze particles is set equal to 1.40 (wavelength independent), which is representative for 75 % sulfuric acid (H_2SO_4) at 1.45 μm (Palmer & Williams, 1975).

We describe the sizes of the cloud and haze particles by log-normal distributions, with as parameters the modal radius $r_{\rm g}$ and the variance σ (Knollenberg & Hunten, 1980). For the cloud particles, we use the micron-sized "mode 2" particles, and for the haze particles, the sub-micron sized "mode 1" particles. The cloud particles thus have $r_{\rm g} = 1.05$ μm and $\sigma = 1.21$, and the haze particles, $r_{\rm g} = 0.15$ μm and $\sigma = 1.91$ (Fedorova et al., 2016). The lower cloud region (i.e. below 60 km) should also have particles that are usually referred to as "mode 3" (Knollenberg & Hunten, 1980) with sizes of ~ 4 μm, but we neglect these particles in our model, as the traces they leave in the reflected light are negligible.

Figure 4 shows the phase functions (element P_{11} of the single scattering matrix $\mathbf{P}^{\rm a}$) and the degree of linear polarization for unpolarized incident light (i.e. $-P_{21}/P_{11}$) of the cloud and the haze particles at $\lambda = 1.45$ μm. Single scattering matrix $\mathbf{P}^{\rm m}$ of the CO_2 gas is the anisotropic Rayleigh scattering matrix described by Hansen and Travis (1974), and P_{11} and $-P_{21}/P_{11}$ of this matrix are also shown in Fig. 4. The curves for the cloud particles have strong angular features because they are large compared to the wavelength.

The single scattering matrix pertaining to an atmospheric layer that contains both aerosol particles and gas is given by

$$\mathbf{P}(\lambda) = \frac{b_{\rm sca}^{\rm m}(\lambda)\mathbf{P}^{\rm m}(\lambda) + b_{\rm sca}^{\rm a}(\lambda)\mathbf{P}^{\rm a}(\lambda)}{b_{\rm sca}(\lambda)} \tag{7}$$

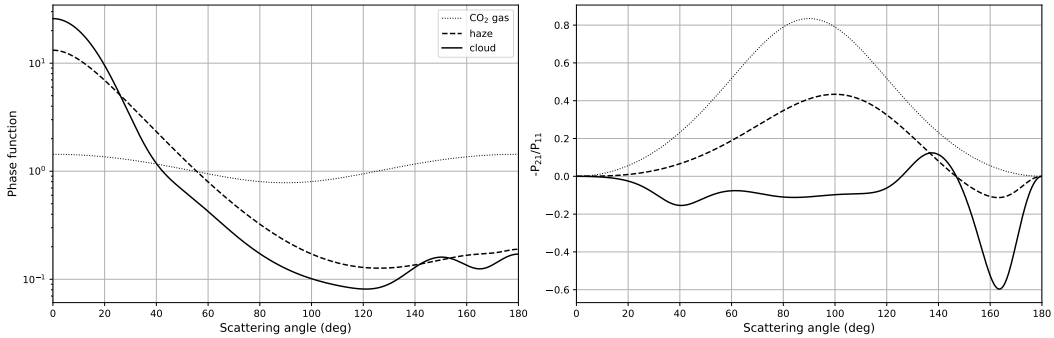

Figure 4. The phase functions (left) and degree of linear polarization (right) for incident unpolarized light that is singly scattered by the cloud (solid lines) or haze (dashed lines) particles at $\lambda = 1.45$ μm, or the CO_2 gas (dotted lines). The phase functions have been normalized such that their average over all scattering directions equals 1.0 (see Hansen & Travis, 1974).

and the single scattering albedo pertaining to this layer by

$$a(\lambda) = \frac{b^{\rm m}_{\rm sca}(\lambda) + b^{\rm a}_{\rm sca}(\lambda)}{b(\lambda)}. \tag{8}$$

We employ two vertical distributions to investigate the influence of aerosol on the flux and polarization signals across the CO_2 absorption bands. In the 'slab model', clouds and hazes have a constant particle number density N_0 (in $\rm cm^{-3}$) between altitudes z_0 and $z_{\rm cut}$. While this model provides easy insight in the influence of the cloud and haze vertical structure on the reflected fluxes and polarization, the scale-height model is more representative of in-situ and remote-sensing measurements (Knollenberg & Hunten, 1980; Fedorova et al., 2016). In the 'scale-height model', a constant vertical particle distribution N_0 is extended from the bottom of the cloud deck, $z_{\rm bot}$, to a threshold altitude $z_{\rm cut}$, above which we use an exponential profile, such that the aerosol number density $N^{\rm a}_j$ (in $\rm cm^{-3}$) in layer i equals

$$N^{\rm a}_i = N_0 \exp\left(-\frac{z_i - z_{\rm cut}}{H}\right) \tag{9}$$

with H the aerosol scale height (in km) and z_i the altitude of the middle of the layer. Hence, N^a_i represents the particle number density at the middle of the layer i. An important parameter in our simulations is the cloud-top altitude $z_{\rm top}$, defined as the altitude at which the total cloud optical thickness (measured from the top of the atmosphere) reaches 1 and depends on the wavelength. Details about the profile and the relation between $z_{\rm bot}$, $z_{\rm cut}$ and $z_{\rm top}$ are given in Appendix B.

3 Results

Given the strong spectral variations of the gaseous absorption cross–section (see Fig. 3), the flux F and degree of polarization P of the sunlight that is reflected by a planet across a gaseous absorption band will show strong spectral variations too. Observing these variations would require a very high spectral resolution. An instrument like SPICAV-IR, for example, has a spectral resolution of ∼0.001 μm in its long-wavelength (1.05 - 1.7 μm) spectral region and a broad instrument response (Korablev et al., 2012), which is not enough to resolve individual lines. To understand flux and/or polarization measurements across gaseous absorption bands, such as those performed by SPICAV-IR, understanding the underlying high-spectral resolution variations due to the numerous CO_2

absorption lines is, however, important. In the following, we will therefore first present and discuss fluxes and polarization of reflected sunlight as functions of the atmospheric absorption optical thickness $\sum b^{\rm m}_{\rm abs}$ (Sect. 3.1) and then as functions of the wavelength given a spectral resolution of 0.001 μm (Sect. 3.2), similar to that of SPICAV-IR.

3.1 *F* and *P* as functions of the absorption optical thickness

Figure 5 shows the reflected F and P as functions of the atmospheric absorption optical thickness $\sum b^{\rm m}_{\rm abs}$. The vertical distribution of the gaseous absorption is that at $\lambda = 1.425$ μm, where, to cover a $\sum b^{\rm m}_{\rm abs}$ range from zero to 10^4, we multiply $b^{\rm abs}_{\rm m}$ (at 1.425 μm) of each layer with a constant. At these long wavelengths, the total gas scattering optical thickness is ~ 0.38 (see Fig. 3). The cloud and haze optical thicknesses are 30 and 0.1, respectively, and are modeled as slabs, (H is thus zero for both). The viewing direction is nadir ($\theta = 0°$) and the solar zenith angle θ_0 is 30°, 45°, or 60°. Angle $\phi - \phi_0$ is undefined and set to 0°.

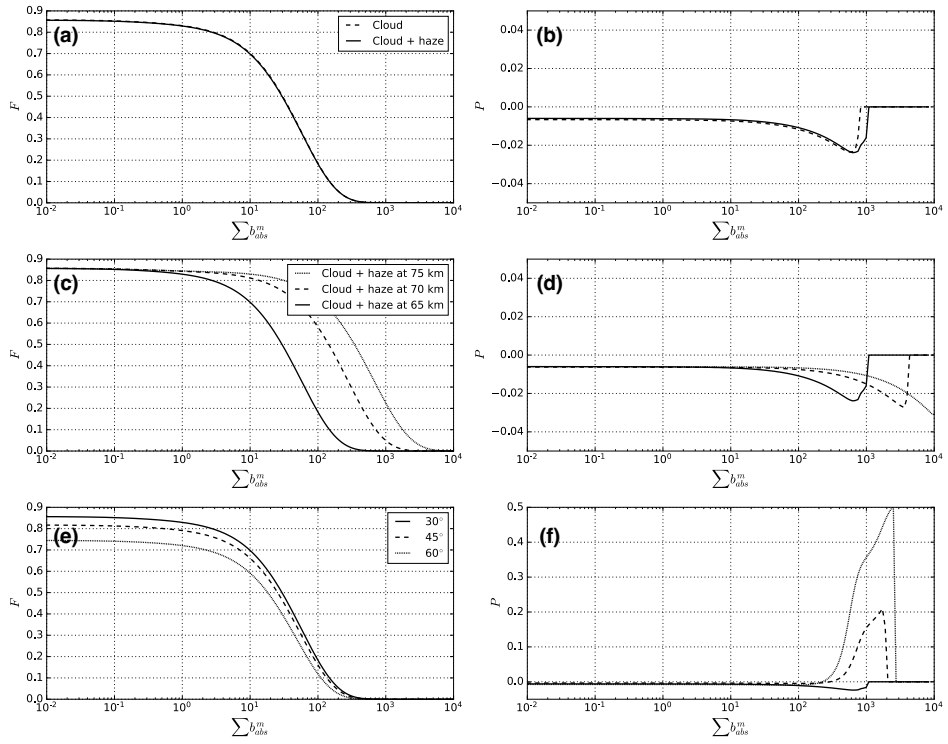

Figure 5. Reflected flux F (left) and degree of polarization P (right) as functions of the atmospheric absorption optical thickness $\sum b^{\rm m}_{\rm abs}$. The viewing direction is nadir ($\theta = 0°$). The clouds and hazes are of the 'slab model'. Top: An atmosphere with a cloud with $b^{\rm a} = 30$, with its top at 65 km (solid lines); an atmosphere with a $b^{\rm a} = 30$ cloud with its top at 65 km, and an overlying $b^{\rm a} = 0.1$ haze (dashed lines). The solar zenith angle θ_0 is 30°. Middle: An atmosphere with a $b^{\rm a} = 30$ cloud and an overlying $b^{\rm a} = 0.1$ haze. The cloud top is at 65 km (dotted lines), 70 km (dashed lines), or 75 km (solid lines). The haze top extends 2 km above the cloud top in each case. The solar zenith angle is 30°. Bottom: An atmosphere with a $b^{\rm a} = 30$ cloud with its top at 65 km, and an overlying $b^{\rm a} = 0.1$ haze with its top at 67 km. The solar zenith angle θ_0 is 30° (solid lines), 45° (dashed lines), or 60° (dotted lines). When at the largest values of $\sum b^{\rm m}_{\rm abs}$, P suddenly drops to zero, the signal is below the computational accuracy.

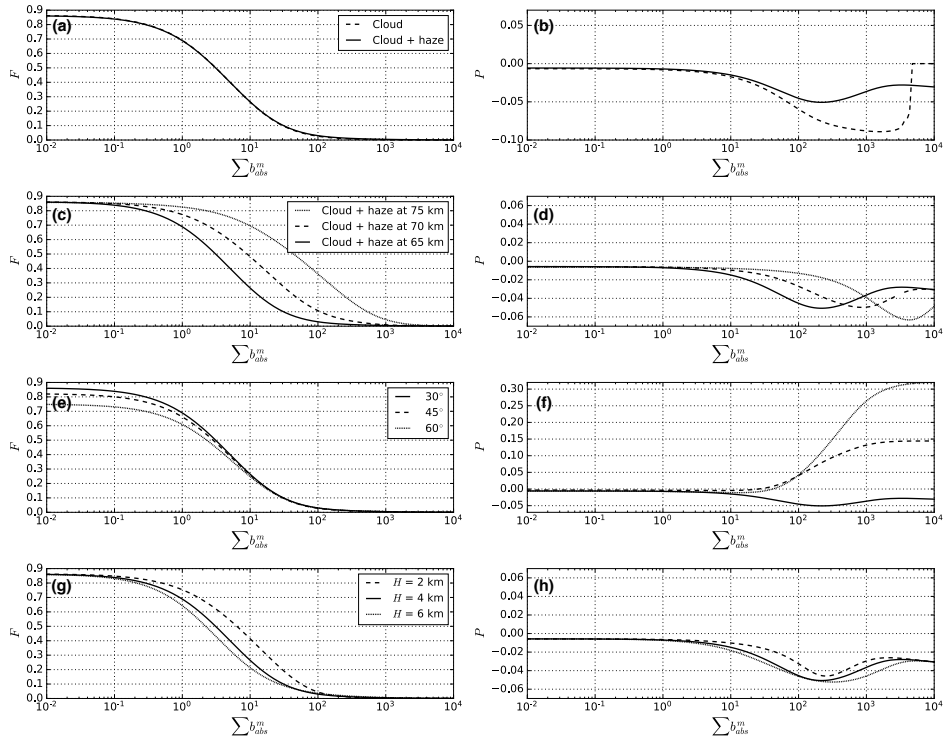

Figure 6. Similar to Fig. 5, except with the cloud and haze particle vertical distribution described by a non-zero scale height H. In rows 1-3, H = 4 km, and in row 4, H of the cloud is varied, while the effective cloud top altitude is at 65 km. The haze scale height is 4 km in all rows.

As can be seen in Fig. 5, increasing $\sum b^{\rm m}_{\rm abs}$ decreases F for all model atmospheres and illumination angles θ_0. The top row shows that adding the haze ever so slightly decreases F as compared to the cloudy atmosphere, probably because it scatters more light down, into the cloud. As can be seen in the middle row, at these long wavelengths, there is little gaseous scattering above the cloud and haze, hence the cloud and haze top altitude has virtually no effect on F at small values of $\sum b^{\rm m}_{\rm abs}$. However, in the presence of absorption, the higher the cloud and haze, the less CO_2 gas above it, and the higher F at a given value of $\sum b^{\rm m}_{\rm abs}$. The bottom row shows that with increasing θ_0, F decreases at a given value of $\sum b^{\rm m}_{\rm abs}$ as the incident flux per m^2 at the top of the atmosphere decreases, and as the path-length through the atmosphere increases. In addition, the flux of light that is singly scattered by the cloud particles decreases with increasing θ_0 and thus decreasing single scattering angle (cf. Fig. 4).

An increase in $\sum b^{\rm m}_{\rm abs}$ can increase or decrease P, as can be seen in the right column of Fig. 5. The continuum P depends strongly on the single and multiple scattering polarization of the particles that scatter most of the light (cf. Fig. 4). This explains the small difference (~ 0.2 %) in the continuum P for the two atmosphere models (top row) since scattering is primarily by the clouds, and the lack of a difference in the continuum P for the three different cloud and haze altitudes (middle row). With increasing $\sum b^{\rm m}_{\rm abs}$, the amount of multiple scattering decreases, and the altitude where P of the reflected light is determined, increases. This means that P of the reflected light is increasingly determined by the single scattering properties of the particles at increasing altitudes. With the cloudy atmosphere, P of the single scattering by the cloud particles

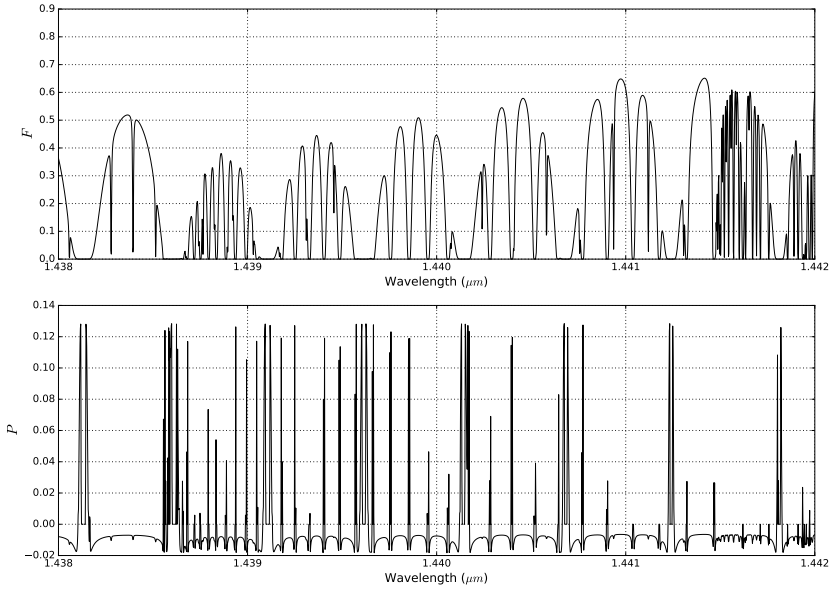

Figure 7. High–spectral resolution F and P of light reflected by an atmosphere with a cloud and haze, with the cloud top altitude at 65 km, H= 4 km, and $\theta_0 = 30°$. This is similar to the slab model atmosphere case in Fig. 8 (solid lines) computed using ck-distribution method.

dominates, while with the cloudy and hazy atmosphere, multiple scattering by cloud particles with some haze dominates at small values of $\sum b^{\rm m}_{\rm abs}$. At large values of $\sum b^{\rm m}_{\rm abs}$, the single scattering by the haze particles dominates. Increasing θ_0 (bottom row), decreases the single scattering angle and changes P of the singly scattered light accordingly (cf. Fig. 4), increasing the difference between P singly scattered by the haze particles and the cloud particles.

Figure 6 is similar to Fig. 5, except here, the clouds and hazes have a non-zero scale height H. Apart from the plots in the bottom row, $H =$ 4 km. With a non-zero scale-height, the curves for F are very similar to those with the slab model case. For P, however, the change of the polarization with increasing value of $\sum b^{\rm m}_{\rm abs}$ is smoother due to the presence of cloud and haze particles high up in the atmosphere. The presence of cloud and haze particles in the high atmospheric layers also influences P at the largest values of $\sum b^{\rm m}_{\rm abs}$, as compared to the slab model where these higher layers only contained gaseous molecules. The bottom row of Fig. 6 shows the effect of changing H while keeping the cloud top at the same altitude: with increasing H, the higher layers contain more cloud particles, and the lower layers less. At intermediate values of $\sum b^{\rm m}_{\rm abs}$, the reflected light has mostly been scattered in those lower layers, and increasing H thus decreases F and $|P|$. At the highest values of $\sum b^{\rm m}_{\rm abs}$, the reflected light has been scattered in the highest layers, and increasing H increases F (this is very hard to see in Fig. 6), and decreases $|P|$ (as compared to that of light scattered by gaseous molecules).

3.2 *F* and *P* as functions of the wavelength

Figure 7 shows computed high spectral resolution spectra ($\Delta\lambda \sim$ 0.002 nm) of the reflected F and P. The atmosphere contains both cloud and haze particles, with optical thicknesses of 30 and 0.1, respectively, the cloud and haze scale height H is 4 km and the cloud top is at 65 km. Solar zenith angle θ_0 is 30°. The numerous fine lines following the absorption lines of CO_2 (cf. Fig. 3) can clearly be seen, with F decreasing with

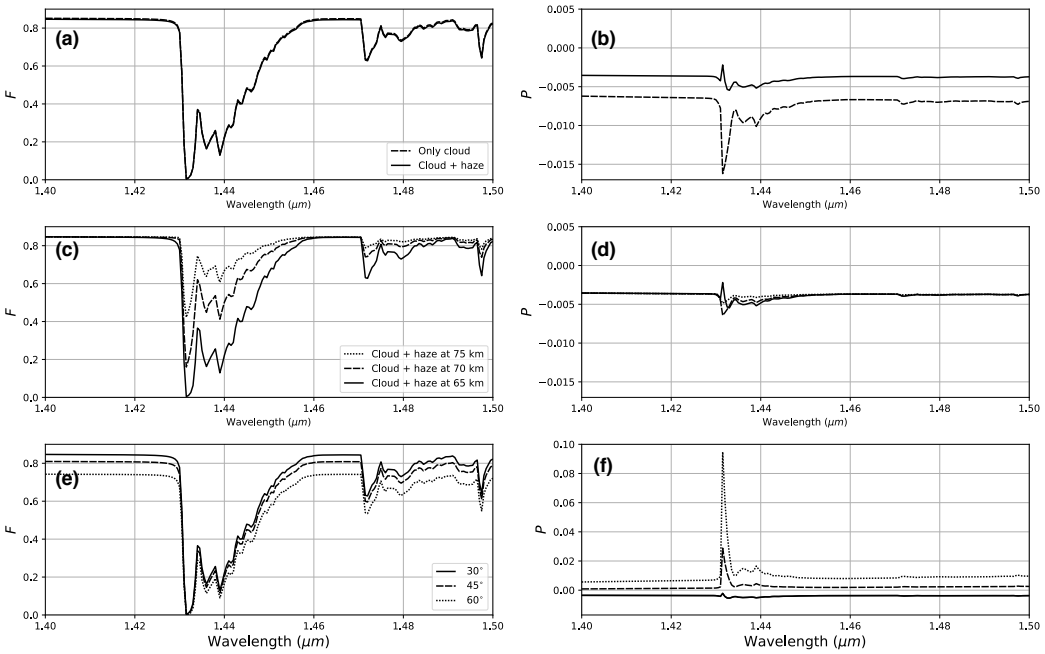

Figure 8. Reflected flux F (left) and P (right) as functions of λ for the same atmosphere models and solar zenith angles as in Fig. 5.

increasing $\sum b_{\rm abs}^{\rm m}$. With increasing absorption, P becomes more negative (it thus increases in absolute value), while for the largest values of $\sum b_{\rm abs}^{\rm m}$, P changes from negative to positive, and shows sharp peaks.

While our simulations above show that very high-spectral resolution measurements of F and especially P could provide valuable information on the vertical distribution of clouds and hazes, we next integrate reflected fluxes[1] across a hypothetical instrumental spectral response function to show what an instrument with a finite spectral resolution would measure, using a box shaped spectral response function (to avoid introducing too many free parameters) with a width of 0.001 μm.

Figure 8 shows F and P for the model atmospheres (with clouds and hazes modeled as slabs) and θ_0 as used in Fig. 5. Like in Fig. 5, the curves of F for the atmosphere with only clouds and the atmosphere with clouds and hazes (top row) are virtually the same. The haze does influence P across the band: while with only a cloud, P in the deepest part of the band is relatively large and negative due to the scattering by the cloud particles, the haze particles decrease $|P|$ as they add positively polarized singly scattered light (cf. Fig. 4).

Increasing the cloud top altitude (middle row) strongly decreases F inside the band as less CO_2 is located above the cloud. Because with increasing cloud top, there are more cloud particles in higher atmospheric layers, P becomes slightly more negative, due to the single scattering polarization signature of the cloud particles. And for the highest cloud and haze, the band structure seems to disappear because of the strongly decreased

[1] We integrate F, Q, and U, and compute P from the integrated fluxes.

amount of CO_2 above the scattering particles. Increasing the solar zenith angle θ_0 (bottom row) decreases F in the continuum and across the band, but only slightly in the deepest part of the band. Increasing θ_0 changes the continuum P from negative (parallel to the reference plane) to positive (perpendicular to the plane), and strongly increases P inside the absorption band, as more light is scattered by the gas above the clouds over a single scattering angle that decreases from 150° ($\theta_0 = 30°$) to 120° ($\theta_0 = 60°$).

Figure 9 shows F and P across the same spectral region with the same spectral response function, except for the scale-height atmosphere models. While the overall behaviour of F across the band is similar to that with the slab model cloud and haze (Fig. 8), the more extended vertical distribution of the cloud and haze particles strongly influences the width of the band in F (second row). Increasing the scale height H (bottom row) slight deepens the band in F due to more absorption by gas above the cloud. The behaviour of P for the scale-height models is also similar to that for the slab models, except that the presence of haze and cloud particle higher up into the atmosphere influences P across a wider range of absorption optical thicknesses, leaving stronger features across the band.

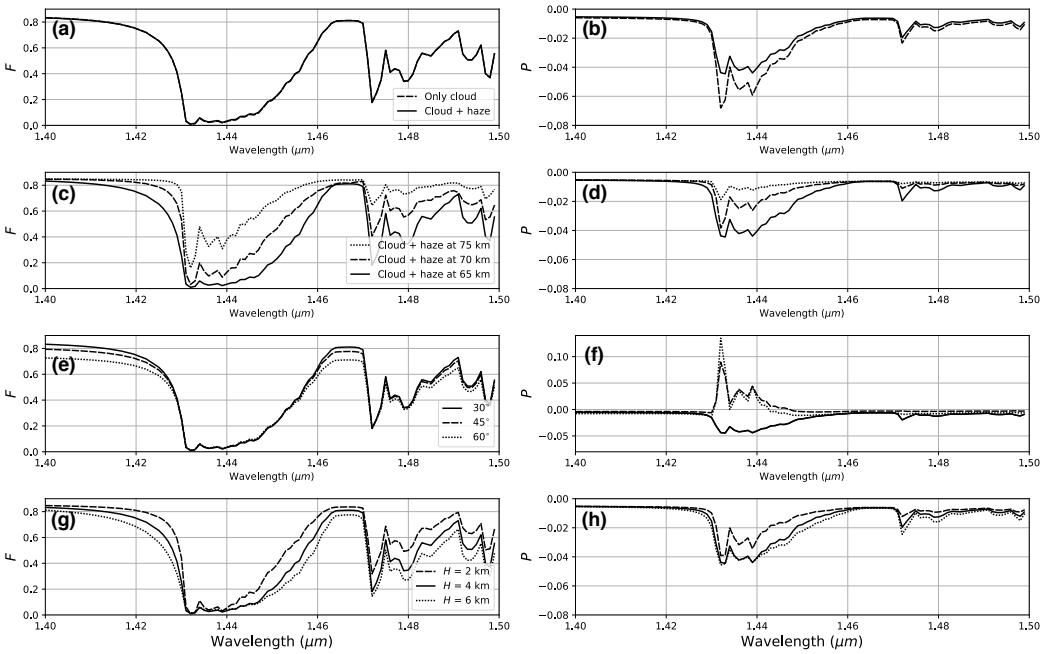

Figure 9. Similar to Fig. 8, except for the scale height models. All models have $z_{\text{top}} = 65$ km, except second row.

Changes in the scale height of the haze layer appear to have negligible effects on both F and P. Changing this scale height between 2 and 6 km while keeping the cloud top altitude and scale height constant, led to changes less than 0.5% in both F and P at least for haze optical thicknesses of 0.1 to 0.8. To investigate the effect of b_{cloud} on F and P, we changed b_{cloud} from 30 to 40 by adding cloud particles to the lower part of the cloud. This appeared to have a negligible effect on F and P inside the absorption band, as expected, because for F, b_{cloud} is already in the convergence regime, while P inside the band is primarily determined by the upper cloud and haze particle properties.

4 The influence of the spectral response function

The determination of the composition, structure, and variability of Venus's cloud and haze layers is important for understanding the physical processes that sustain them and the planet's current climate. Determining the cloud top altitude using only total flux measurements across CO_2 absorption bands has limitations such as having to assume the scale height of the cloud layer. Constraining the properties of the overlaying haze layer, such as its optical thickness and particle properties, from total flux measurements is difficult because the haze optical thickness is small.

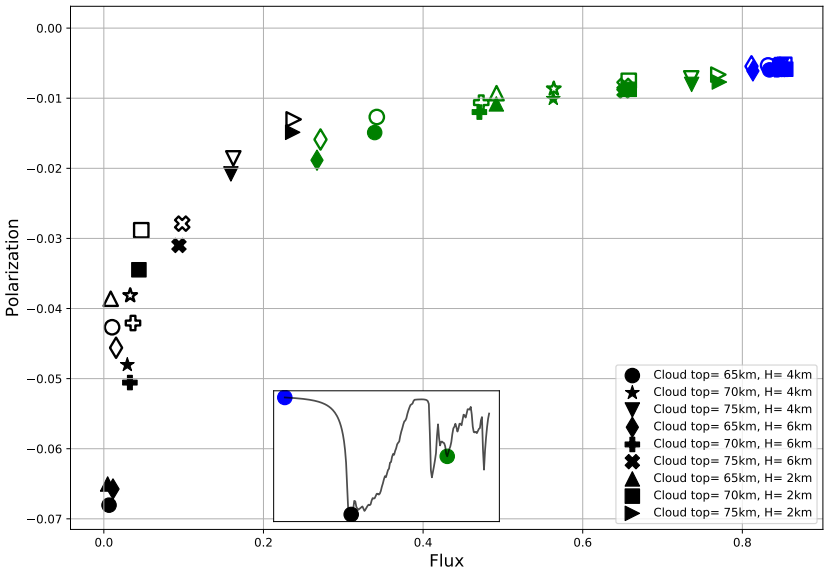

Figure 10. Scatter plot of P versus F for all the scale-height model atmospheres in three spectral intervals covering the absorption band (see the subplot): the continuum in blue, the deepest part of the band in black, an intermediate part of the band in green. The filled markers indicate model atmospheres with only clouds and the open markers model atmospheres with clouds and a haze layer with $b^{\mathrm{a}} = 0.1$.

Figure 10 shows our computed values for F and P in three different parts of the absorption band for different model atmospheres. The figure clearly shows that P in the deepest part of the band is more sensitive to the presence of haze (open symbols) than F is: adding haze to a cloudy model atmosphere changes P while keeping F more or less constant. Polarimetry across an absorption band would thus help to retrieve information about the hazes. It helps here that in the wavelength range and scattering angle range considered, the single scattering polarization of the cloud particles is negative while that of the haze particles is positive, similar to Rayleigh scatterers.

However, the effect of the haze on P is strongest in the deepest part of the band, where F is very small, potentially leading to very small signal to noise ratios. Another important issue would be the instrumental spectral resolution. In Fig. 10, the box-shaped response function has a width of 1 nm. The effect of a different width is shown in Fig. 11. Indeed, increasing the width, decreases the depth of the absorption band both in F and in P, severely limiting the possibilities for retrieving haze properties or atmospheric vertical structure. A low-noise, high-spectral resolution instrument would thus be needed to fully use P across an absorption band.

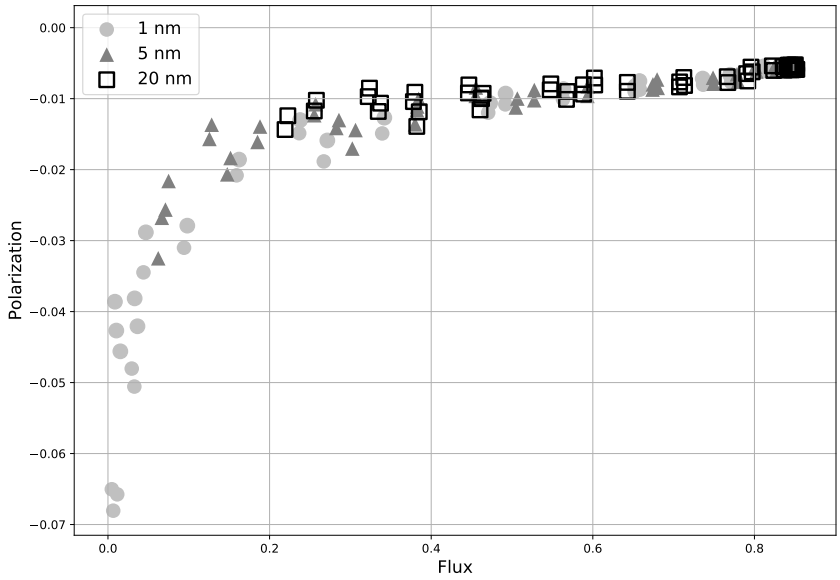

Figure 11. Similar to Fig. 10, except for different widths of a box-shaped instrumental response function: 1 nm (light grey circle), 5 nm (dark grey triangle), and 20 nm (box). Each given type of symbol is used for all the model atmospheres detailed in Fig. 10.

5 Conclusions

We have presented numerical simulations of the flux F and degree of (linear) polarization P of light reflected locally by the atmosphere of Venus, in the wavelength range between 1.4 - 1.5 μm which contains a strong CO_2 absorption band.

The cloud top altitude has a strong influence on both F and P within the absorption band. This added information contained in the degree of polarization of the reflected light can be used to remove the existing degeneracy between the effects of cloud top and scale heights as our results show that polarization adds to the information provided by total flux. This could lead to a possible retrieval of both the cloud top and scale height parameters. Similar case studies for Earth have been performed in the past which use both flux and degree of polarization to narrow down the degeneracy's inherent in certain parameter retrievals (see Mishchenko and Travis (1997) for details).

The haze on top of the clouds has a negligible impact on F, but does influence P. Our simulations show that haze layers with b^{a} greater than 0.1 causes a change of more than 2 % for illumination geometries $> 30°$. This signal in polarization increases with increasing solar zenith angle (in nadir viewing angle) due to the single scattering properties of the haze particles. Such variability is well within the detectable range of an instrument such as SPICAV (Rossi et al., 2015).

Our simulations show a significant effect of the vertical distribution of cloud and haze particles on P, and less on F. This sensitivity of P is due to the underlying differences in the amount of scattering (single or multiple) in the atmosphere and the dependence of P on the local single scattering properties of the cloud and haze particles. Spectropolarimetry would thus provide additional information on the vertical distribution of aerosol, as compared to only total flux measurements.

The spectral resolution of measurements of F and especially P across a gaseous absorption band strongly determines the band strength and information content: the higher the resolution, the stronger the features and the more information.

In our simulations, we have assumed a log-normal particle size distribution, following in-situ measurements by the Pioneer Venus LCPS (Knollenberg & Hunten, 1980). Variations in particle size and vertical distribution will influence P of the reflected light. The influence of the spatial variability of sulphuric-acid concentration (Cottini et al., 2012) and therefore the variability of the refractive index, which is assumed to be constant in our models, on P across the absorption band, is another parameter that would be interesting to investigate.

We will use the knowledge gained from the study presented here to perform retrievals using existing data as measured by SPICAV on Venus Express (Fedorova et al., 2016; Rossi et al., 2015; Korablev et al., 2012) with the aim to improve upon Venus cloud top altitudes, cloud scale heights, and haze properties as derived from other data sets with other methods.

Acknowledgments
Funding support for this research was provided by NWO, the Netherlands Organization for Scientific Research. We shall provide access to the data for this work through the 4TU.ResearchData repository (https://researchdata.4tu.nl) at the time of acceptance.

References

Bertaux, J.-L., Nevejans, D., Korablev, O., Villard, E., Quémerais, E., Neefs, E., ... others (2007). Spicav on venus express: Three spectrometers to study the global structure and composition of the venus atmosphere. *Planetary and Space Science*, *55*(12), 1673–1700.

Bideau-Mehu, A., Guern, Y., Abjean, R., & Johannin-Gilles, A. (1973). Interferometric determination of the refractive index of carbon dioxide in the ultraviolet region. *Optics Communications*, *9*(4), 432–434.

Cottini, V., Ignatiev, N., Piccioni, G., Drossart, P., Grassi, D., & Markiewicz, W. (2012). Water vapor near the cloud tops of venus from venus express/virtis dayside data. *Icarus*, *217*(2), 561–569.

de Haan, J. F., Bosma, P., & Hovenier, J. (1987). The adding method for multiple scattering calculations of polarized light. *Astronomy and Astrophysics*, *183*, 371–391.

De Rooij, W., & Van der Stap, C. (1984). Expansion of mie scattering matrices in generalized spherical functions. *Astronomy and Astrophysics*, *131*, 237–248.

Drossart, P., Piccioni, G., Adriani, A., Angrilli, F., Arnold, G., Baines, K., ... others (2007). Scientific goals for the observation of venus by virtis on esa/venus express mission. *Planetary and Space Science*, *55*(12), 1653–1672.

Fedorova, A., Marcq, E., Luginin, M., Korablev, O., Bertaux, J.-L., & Montmessin, F. (2016). Variations of water vapor and cloud top altitude in the venus mesosphere from spicav/vex observations. *Icarus*, *275*, 143–162.

Forbes, F., & Fymat, A. (1974). Astronomical fourier spectropolarimetry.

Fu, Q., & Liou, K. (1992). On the correlated k-distribution method for radiative transfer in nonhomogeneous atmospheres. *Journal of the Atmospheric Sciences*, *49*(22), 2139–2156.

Gordon, I. E., Rothman, L. S., Hill, C., Kochanov, R. V., Tan, Y., Bernath, P. F., ... others (2017). The hitran2016 molecular spectroscopic database. *Journal of Quantitative Spectroscopy and Radiative Transfer*, *203*, 3–69.

Hansen, J. E., & Hovenier, J. (1974). Interpretation of the polarization of venus. *Journal of the Atmospheric Sciences*, *31*(4), 1137–1160.

Hansen, J. E., & Travis, L. D. (1974). Light scattering in planetary atmospheres. *Space science reviews*, *16*(4), 527–610.

Ignatiev, N., Titov, D., Piccioni, G., Drossart, P., Markiewicz, W., Cottini, V., ... Manoel, N. (2009). Altimetry of the venus cloud tops from the venus express observations. *Journal of Geophysical Research: Planets*, *114*(E9).

Kawabata, K., Coffeen, D., Hansen, J., Lane, W., Sato, M., & Travis, L. (1980). Cloud and haze properties from pioneer venus polarimetry. *Journal of Geophysical Research: Space Physics*, *85*(A13), 8129–8140.

Kemp, J. C., Henson, G., Steiner, C., & Powell, E. (1987). The optical polarization of the sun measured at a sensitivity of parts in ten million. *Nature*, *326*(6110), 270.

Knollenberg, R., & Hunten, D. (1980). The microphysics of the clouds of venus: Results of the pioneer venus particle size spectrometer experiment. *Journal of Geophysical Research: Space Physics*, *85*(A13), 8039–8058.

Korablev, O., Fedorova, A., Bertaux, J.-L., Stepanov, A., Kiselev, A., Kalinnikov, Y. K., ... others (2012). Spicav ir acousto-optic spectrometer experiment on venus express. *Planetary and Space Science*, *65*(1), 38–57.

Lacis, A., Hansen, J., & Sato, M. (1992). Climate forcing by stratospheric aerosols. *Geophysical Research Letters*, *19*(15), 1607–1610.

Lacis, A., & Oinas, V. (1991). A description of the correlated k distribution method for modeling nongray gaseous absorption, thermal emission, and multiple scattering in vertically inhomogeneous atmospheres. *Journal of Geophysical Research: Atmospheres*, *96*(D5), 9027–9063.

Mishchenko, M. I., & Travis, L. D. (1997). Satellite retrieval of aerosol properties over the ocean using polarization as well as intensity of reflected sunlight. *Journal of Geophysical Research: Atmospheres*, *102*(D14), 16989–17013.

Palmer, K. F., & Williams, D. (1975). Optical constants of sulfuric acid; application to the clouds of venus? *Applied Optics*, *14*(1), 208–219.

Rossi, L., Marcq, E., Montmessin, F., Fedorova, A., Stam, D., Bertaux, J.-L., & Korablev, O. (2015). Preliminary study of venus cloud layers with polarimetric data from spicav/vex. *Planetary and Space Science*, *113*, 159–168.

Rossi, L., & Stam, D. M. (2018). Circular polarization signals of cloudy (exo) planets. *arXiv preprint arXiv:1805.08686*.

Seiff, A., Schofield, J., Kliore, A., Taylor, F., Limaye, S., Revercomb, H., ... Marov, M. Y. (1985). Models of the structure of the atmosphere of venus from the surface to 100 kilometers altitude. *Advances in Space Research*, *5*(11), 3–58.

Stam, D., De Haan, J., Hovenier, J., & Stammes, P. (1999). Degree of linear polarization of light emerging from the cloudless atmosphere in the oxygen a band. *Journal of Geophysical Research: Atmospheres*, *104*(D14), 16843–16858.

Stam, D., De Haan, J., Hovenier, J., & Stammes, P. (2000). A fast method for simulating observations of polarized light emerging from the atmosphere applied to the oxygen-a band. *Journal of Quantitative Spectroscopy and Radiative Transfer*, *64*(2), 131–149.

Stam, D., & Hovenier, J. (2005). Errors in calculated planetary phase functions and albedos due to neglecting polarization. *Astronomy & Astrophysics*, *444*(1), 275–286.

Svedhem, H., Titov, D., Taylor, F., & Witasse, O. (2009). Venus express mission. *Journal of Geophysical Research: Planets*, *114*(E5).

Titov, D., Svedhem, H., Koschny, D., Hoofs, R., Barabash, S., Bertaux, J.-L., ... others (2006). Venus express science planning. *Planetary and Space Science*, *54*(13-14), 1279–1297.

Travis, L. D. (1979). *Imaging and polarimetry with the pioneer venus orbiter cloud photopolarimeter* (Vol. 0183). Retrieved from `https://doi.org/10.1117/12.957426` doi: 10.1117/12.957426

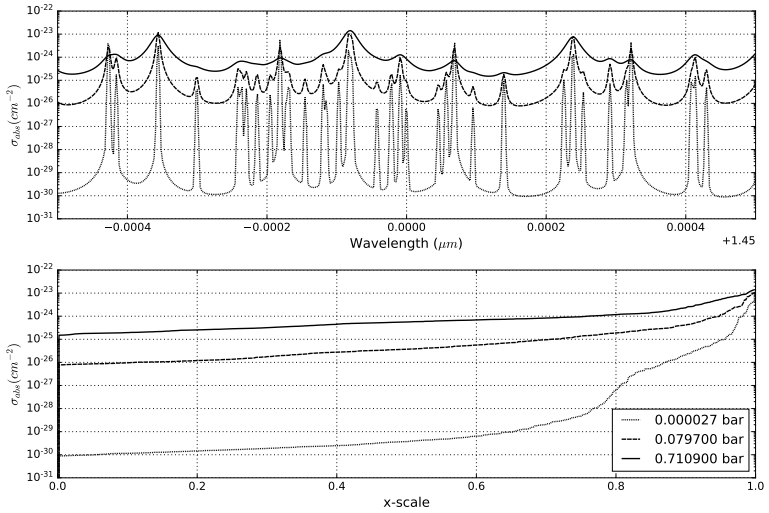

Figure A1. Top: CO_2 absorption cross-sections at three pressure levels as functions of the wavelength. Bottom: the corresponding sorted cross-sections on a cumulative distribution scale.

Appendix A The accuracy of the correlated *k*-distribution method applied to Venus's CO_2 bands

In this paper, we use the correlated k-distribution method (c*k*-method), for the computations of reflected sunlight across CO_2 absorption bands (Lacis & Oinas, 1991; Stam et al., 2000). In this method, the highly wavelength dependent absorption cross-sections ($\sigma_{\rm abs}$) across a given spectral interval (see Fig. A1 top) are re-arranged based on their strength, resulting in a relatively smooth function (see Fig. A1 bottom) that describes the same variation in absorption cross-sections as the original absorption cross-section spectrum, but that can be represented with far less radiative transfer computations than the original spectrum. Because the spectral information about the absorption cross-sections is lost in this process, the c*k*-method assumes that these cross-sections are correlated in wavelength space, which is not necessarily the case due to the dependence of absorption cross-section spectra on the ambient pressure and temperature (see Fig. A1). We have analyzed the errors in our computed fluxes and polarization due to using the c*k*-method by comparing them with fluxes and polarization computed using line-by-line computations, following the analysis by Stam et al. (2000) for sunlight reflected by Earth, except for Venus.

For the comparison of line-by-line results with c*k*-method results, we use a spectral resolution of 1 nm and a box-shaped response function. We thus convolve the computed high-spectral resolution line-by-line total and polarized fluxes with the response function, and apply the c*k*-method to the same, 1 nm wide spectral bins, using Gauss-Legendre integration for each bin, with 20 Gaussian abscissae. The errors also depend on the number of Gaussian abscissae and for this 'slab' model case, we found that there was not a significant improvement with an increase in abscissae. Fig. A2 shows examples of computed total fluxes F and degrees of polarization P. The bottom row of this figure shows the errors in F and P defined as by Stam et al. (2000), i.e.

$$\Delta F = (F_{\rm ck} - F_{\rm lbl})/F_{\rm lbl} \quad \text{(A1)}$$

$$\Delta P = \sqrt{(P_{\rm ck} - P_{\rm lbl})^2}. \quad \text{(A2)}$$

We find that with the ck-method, F is higher, and P is larger than with the line-by-line method. The errors increase with increasing θ_0 and are observing geometry dependent, as can be seen in bottom row of Fig. A2 where the errors increase slightly for 60°. For θ_0 lower than 60°, relative error is lower than 12 % in flux and absolute error smaller than 0.1 % in polarization. The errors also depend on the vertical distribution. For an atmosphere with scale height, the absolute errors in polarization increase to $\sim$ 3 %. This is because of the higher amount of scattering in the upper atmospheric layers, which leads to larger errors as compared to the slab model due to the correlation assumption.

To investigate the errors, we plot the $\sigma_{\rm abs}$ for a few sample atmospheric layers at $\lambda = 1.4453$ μm showing significant errors. Fig. A3 shows a 1 nm width bin for three atmospheric layers in the regions containing clouds. It is evident that a substantial amount of absorption lines are uncorrelated in the spectral domain, due to which the scattering effects in these layers are not well represented by ck-distribution approximation. Finally we note that despite these errors in the absorption bands due to high scattering by cloud and haze, our interpretation of the results do not change. To assess whether this method can be used during retrievals of cloud and haze parameters, we intend to elaborate on the error sources further in the future.

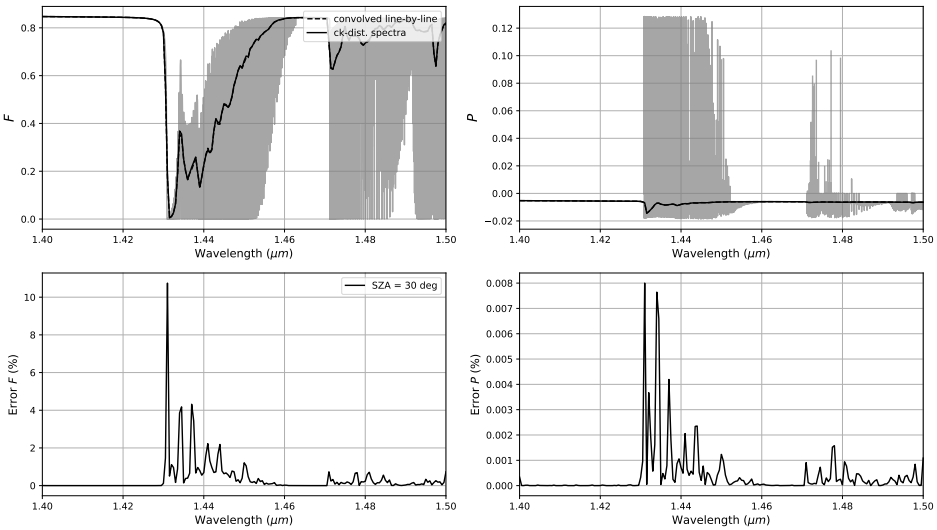

Figure A2. The flux F and degree of polarization P as computed using the line-by-line method, before and after convolution with the instrument response function, and the ck-method (top row). For these computations, $\theta_0 = 30°$ and $\theta = 0°$. Errors due to using the ck-method (bottom row) for $\theta = 0°$ and $\theta_0 = 30°$ or 60°. The atmosphere is a 'slab' model with a cloud top at 65 km and haze with optical thickness 0.1.

Appendix B Aerosol vertical distribution

Here, we outline our computation method of the number densities of aerosol (cloud or haze) particles in the atmospheric layers. Figure B1 shows an example of an aerosol vertical distribution with both a cloud and a haze. In the bottom part of the cloud, starting at altitude $z_{\rm bot}$, the particle number density is constant. Above altitude $z_{\rm cut}$, it decreases exponentially with scale height H, until 76 km, above which, there are no cloud particles. The altitude of the cloud top, $z_{\rm top}$, is defined as the altitude where the cloud optical thickness equals 1 measured from the top of the atmosphere (see below). The par-

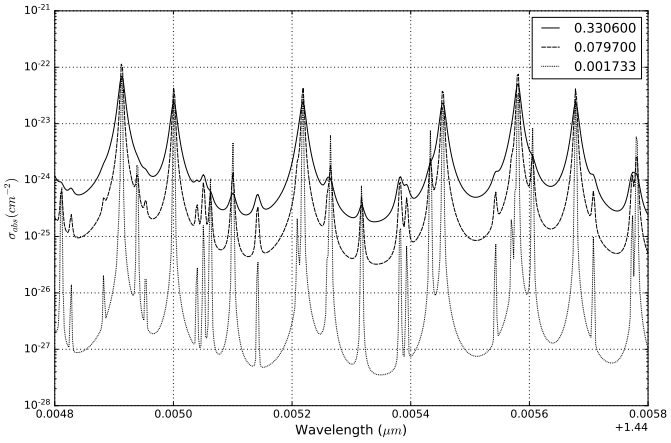

Figure A3. The absorption cross-section spectrum at three different pressure levels (in bars) across the spectral region where the largest errors due to using the ck-method occur (see Fig. A2). The non-correlation between the three curves corresponding to the different pressures can be seen for numerous absorption peaks.

ticle number density of the haze is chosen to decrease exponentially from the bottom upwards.

The aerosol number density, N^a, in a given atmospheric layer, is equal to $k_{\rm ext}/\sigma_{\rm ext}$, where $k_{\rm ext}$ is the (wavelength dependent) extinction coefficient in the layer, and $\sigma_{\rm ext}$ the (wavelength dependent) extinction cross-section of the aerosol. According to Fedorova et al. (2016), $k_{\rm ext} = 2$ km^{-1} in the bottom part of the clouds and across the wavelength region between 1.4 and 1.5 μm. For a log-normal size distribution for the spherical cloud particles, with $r_{\rm g} = 1.05$ μm and $\sigma = 1.21$ and a refractive index of 1.400, we then find $\sigma_{\rm ext} = 18.889 \cdot 10^{-8}$ cm^2, and $N^a = N_0 = 108$ cm^{-3} in the bottom part of the clouds, thus between $z_{\rm bot}$ and $z_{\rm cut}$.

Above altitude $z_{\rm cut}$, the particle number density in layer i, with altitude z_i in the middle of the layer, is then given by

$$N_i^a = N_0 \exp^{-\frac{z_i - z_{\rm cut}}{H}}, \tag{B1}$$

with H the scale height (e.g. in km), the value of which we choose ourselves, based on the literature. We also choose the cloud top altitude, $z_{\rm top}$, based on the literature. In order to determine N^a in a layer, we have to determine $z_{\rm cut}$, for which we can use the following equation:

$$\int_{z_{\rm top}}^{\infty} \sigma_0 N_0 \exp(-\frac{z - z_{\rm cut}}{H})\, dz = 1, \tag{B2}$$

with '1' the cloud optical thickness. From this equation, it follows that

$$z_{\rm cut} = z_{\rm top} - H \ln(\sigma_0 N_0 H) \tag{B3}$$

In the equation above, we implicitly assume that $z_{\rm top}$ falls above $z_{\rm cut}$. Whether this assumption holds, depends on H. For our cases, it holds for H between 2 and 6 km. The bottom altitude of the cloud, $z_{\rm bot}$, is determined from the total optical thickness of the cloud, which we take as 30. In our case, $z_{\rm bot} = 47$ km.

The haze layer (see Fig. B1) is located above the cloud layer and extends up to 96 km. The haze particle number density is computed using Eq. B1, assuming a log-normal

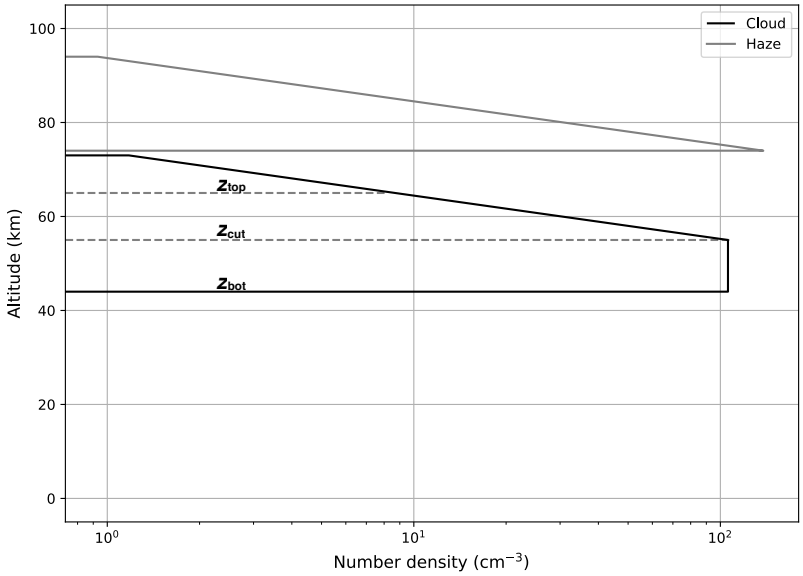

Figure B1. A sample vertical distribution of cloud and haze particles expressed in their number density N^a (cm^{-3}). Both the cloud and the haze have a scale height H of 4 km. The optical thicknesses of the cloud and the haze are 30 and 0.1, respectively. The various altitudes $z_{\rm top}$, $z_{\rm cut}$, and $z_{\rm bot}$ are explained in the text.

size distribution with $\sigma_0 = 0.161 \cdot 10^{-8}$ cm^2 (this is assumed to be wavelength independent). For a given value of H, N_0 is chosen such that the total haze optical thickness equals 0.1.